

# Ground- and Excited-State Pinched Cone Equilibria in Calix[4]arenes Bearing Two Perylene Bisimide Dyes

Catharina Hippus,<sup>†</sup> Ivo H. M. van Stokkum,<sup>‡</sup> Ennio Zangrando,<sup>§</sup> René M. Williams,<sup>\*||</sup> Michael Wykes,<sup>⊥</sup> David Beljonne,<sup>⊥</sup> and Frank Würthner<sup>\*,†</sup>

*Institut für Organische Chemie and Röntgen Research Center for Complex Material Systems, Universität Würzburg, Am Hubland, D-97074 Würzburg, Germany, Department of Physics and Astronomy, Vrije Universiteit, de Boelelaan 1081, 1081 HV Amsterdam, The Netherlands, Dipartimento di Scienze Chimiche, University of Trieste, Via Licio Giorgieri 1, 34127 Trieste, Italy, Molecular Photonics Group, van't Hoff Institute for Molecular Sciences (HIMS), Universiteit van Amsterdam, Nieuwe Achtergracht 129, WS 1018 Amsterdam, The Netherlands, and Laboratory for Chemistry of Novel Materials, Center for Research in Molecular Electronics and Photonics, University of Mons-Hainaut, Place du Parc 20, 7000 Mons, Belgium*

Received: May 8, 2008; Revised Manuscript Received: June 24, 2008

We report on a series of bis-chromophoric compounds **o2c**, **g2c**, and **r2c**, afforded by linking two identical orange, green, or red perylene bisimide (PBI) units, respectively, through a calix[4]arene spacer unit. The PBI units are characterized by their increasing sterical demand from a planar conformation, which is orange (**o**) colored, via the slightly distorted greenish (**g**) colored form to the strongly distorted derivative, which is red (**r**) colored. An equilibrium between the two possible pinched cone conformations of the calix[4]arene unit is observed for all three compounds, with one conformation showing a  $\pi$ -stacked sandwich arrangement of the PBI units and the second revealing a nonstacked conformation. The amount of the  $\pi$ -stacked conformation in the equilibrium enhances upon decreasing the steric encumbering of the respective PBI unit as well as upon lowering the solvent polarity, thus increasing  $\pi$ - $\pi$  interactions as well as electronic coupling between the PBI units. Accordingly, the presence of the  $\pi$ -stacked calix[4]arene conformation is most pronounced for compound **o2c** in methylenecyclohexane (MCH),  $\text{CCl}_4$ , and toluene, and to a lesser extent for compound **g2c** in MCH. Almost no  $\pi$ -stacked conformation is found for the most sterically demanding red system **r2c**. Molecular modeling studies at the force-field level show that the  $\pi$ -stacked conformations of the least sterically hindered dimmer **o2c** are lower in energy than those of the nonstacked ones in a nonpolar environment, whereas, in polar media, these stabilities are inverted. A quantitative analysis of the excited-state properties has been obtained by UV/vis absorption, steady-state and time-resolved emission, and femtosecond transient absorption spectroscopy. Global and target analysis of the femtosecond transient absorption data is used for probing ground-state populations with excited-state dynamics. The **o2c** molecules in the  $\pi$ -stacked conformation display a distinctly different decay behavior relative to the molecules in the nonstacked conformation. The former population decays via an excimer state, with the latter population decaying through a charge separation process involving the calix[4]arene as a donor.

## Introduction

Calix[4]arenes represent one of the most versatile building blocks in supramolecular chemistry.<sup>1</sup> In addition to widespread applications in molecular recognition, calix[4]arenes have been used as versatile scaffolds to organize functional dye units, such as nonlinear optical dyes,<sup>2</sup> electrophores,<sup>3</sup> and fluorophores.<sup>4</sup> Calix[4]arenes can exist as four conformational isomers in solution, i.e., cone, partial cone, 1,2-alternate, and 1,3-alternate (defined by the orientation of the respective phenolic rings toward each other and the linking methylene bridges; for a structural representation of the four isomers, see Figure S1 in the Supporting Information). The *cone* isomer of calix[4]arenes can be conformationally fixed in solution,<sup>5</sup> but interestingly, the thus rigidified skeleton still reveals some remaining flexibility.

Hence, cone isomers of calix[4]arenes are known to undergo geometric changes that vary the distance between two opposite phenol rings.<sup>6</sup> Accordingly, the averaged  $C_{4v}$  symmetry found for calix[4]arenes in the cone conformation can be interpreted in terms of a rapid interconversion between two equivalent so-called pinched cone isomers showing  $C_{2v}$  symmetry (i.e., showing a geometric arrangement with the two opposite aromatic rings almost parallel, while the other two rings adopt an extended position). However, upon partial substitution of the phenolic units, the two pinched cone conformations are no longer equivalent, and, as a consequence, a shift of the equilibrium toward one favorable conformer is expected, depending on the nature of the substituent and also on interactions between the substituting units.<sup>7</sup>

Among the available classes of functional  $\pi$ -systems, perylene bisimides (PBIs) are outstanding with regards to their fluorescence emission (quantum yields up to unity) and n-type semiconducting properties.<sup>8</sup> They represent important photo- and electroactive building blocks in supramolecular dye chemistry<sup>9–11</sup> with excellent emission properties<sup>12</sup> and high absorption coef-

\* Corresponding author. E-mail: wuerthner@chemie.uni-wuerzburg.de (F.W.); williams@science.uva.nl (R.M.W.).

<sup>†</sup> Universität Würzburg.

<sup>‡</sup> Vrije Universiteit.

<sup>§</sup> University of Trieste.

<sup>||</sup> Universiteit van Amsterdam.

<sup>⊥</sup> University of Mons-Hainaut.

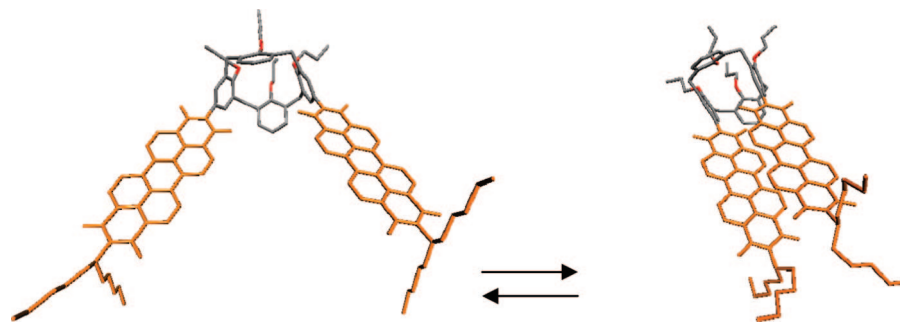
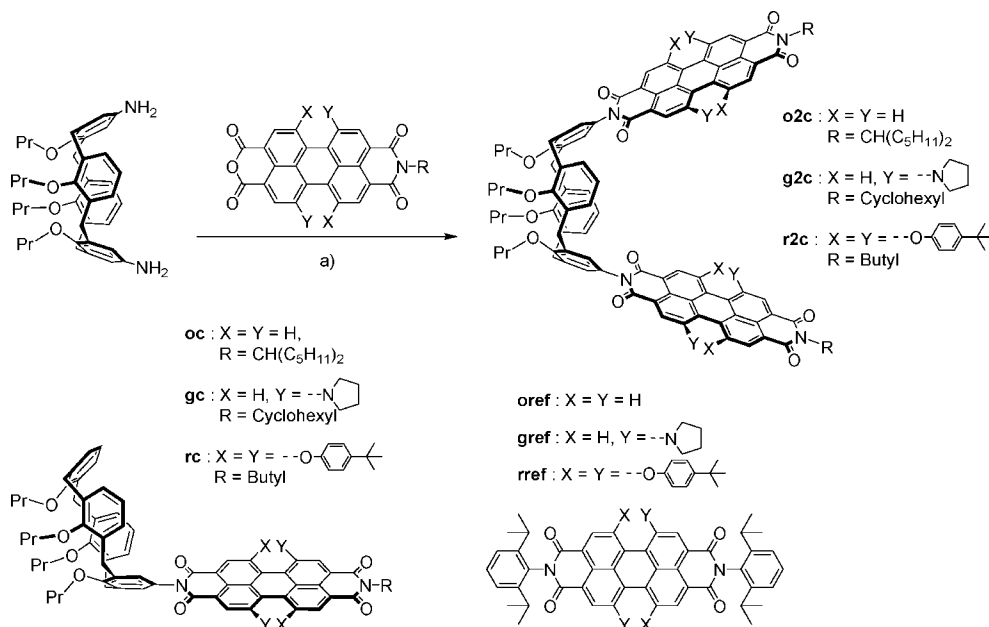


**Figure 1.** Schematic representation of the equilibrium between nonstacked (left) and  $\pi$ -stacked (right) pinched cone conformation of the calix[4]arene unit upon substitution with two orange PBI units (for chemical structure, see compound **o2c** in Scheme 1). Molecular structures obtained from force field calculations (*vide infra* and Supporting Information). Hydrogen atoms have been omitted, and color of the PBI chromophore is applied for clarity.

### SCHEME 1: Synthetic Routes and Chemical Structures of PBI-Calix[4]arene Dimers and Respective Reference Compounds Studied<sup>a</sup>



<sup>a</sup> Reagents and conditions: (a) for compound **o2c**: Zn(OAc)<sub>2</sub>, quinoline, 165 °C, yield 55%; for compound **g2c**: Zn(OAc)<sub>2</sub>, quinoline, 130 °C, yield 32%; for compound **r2c**: Et<sub>3</sub>N, toluene, 125 °C, yield 82%.

ficients and photochemical stability. Different types of intermolecular forces such as hydrogen bonding,  $\pi$ -stacking and metal–ion coordination have been applied to direct the formation of desirable supramolecular structures of PBIs.<sup>8,11,12</sup> PBI dyes and their assemblies find application as functional units in artificial light-harvesting systems,<sup>13</sup> photoinduced electron transfer systems,<sup>14</sup> and organic electronic devices such as organic light emitting diodes (OLEDs),<sup>15</sup> organic thin-film transistors (OTFTs),<sup>16</sup> and solar cells.<sup>17</sup> The PBI chromophore can be easily fine-tuned by proper substitution in the so-called *bay* positions to exhibit quite diverse electronic and optical properties. As such, the classes of phenoxy- (*red*),<sup>18</sup> and pyrrolidino- (*green*)<sup>19</sup> bay-substituted PBIs as well as the core-unsubstituted PBIs (*orange*)<sup>20</sup> are available.

Substitution of two opposing phenolic rings of the calix[4]arene moiety in the *para* positions with PBIs leads to the formation of bis-chromophoric systems. Owing to the intrinsic flexibility of the calix[4]arene spacer unit, two energetically nonequivalent pinched cone species are formed, with one conformer showing  $\pi$ -stacked (PBI residues pointing toward each other), and the other conformer showing nonstacked geometry (PBI residues pointing away from each other). Both species can interconvert,

and a schematic representation of this conformational equilibrium is shown in Figure 1. In contrast to this tweezer-type flexible spacer unit, other examples of bis-chromophoric architectures of dyes are typically limited either to rigid spacer systems without structural flexibility<sup>21,22</sup> or to arrangements of less defined geometry.<sup>23</sup> The interconversion process between the two conformational states and hence the position of the equilibrium should be substantially influenced by the impact of  $\pi$ -stacking between the chromophoric planes, which is governed by solvent effects and by the steric demand of the spacious aromatic systems. As a consequence, proper fine-tuning of all these parameters should enable a controlled adjustment of the conformational equilibrium to afford a switchable bis-chromophoric system. In contrast to systems reported by the group of Swager,<sup>3b,c</sup> where the interactions between electroactive substituents are studied toward a sensing application, the present linkage of calix[4]arenes with PBI units deals with the optical properties of such derivatives.

Accordingly, the work described in this paper elucidates the photophysical behavior of a series of bis-chromophoric compounds **o2c**, **g2c**, and **r2c** afforded by the combination of two orange (**o**), green (**g**), and red (**r**) PBI chromophoric units,

respectively, connected by a calix[4]arene spacer unit via the *N*-imide position of the chromophore. The methodology for the synthesis of calix[4]arene–PBI arrays has been developed before in a collaboration of our and Böhmer's group.<sup>24</sup> Within the series presented here, the three types of PBI substituents used are characterized by their increasing steric demand depending on the bulkiness of the substituents in the *bay* positions, ranging from the *orange* chromophore (hydrogen substituents, with UV/vis absorption maxima at 526 and 490 nm in CH<sub>2</sub>Cl<sub>2</sub>) via the *green* chromophore (pyrrolidino functionalization, showing an UV/vis absorption maximum at 701 nm in CH<sub>2</sub>Cl<sub>2</sub>) to the *red* phenoxy bay-substituted PBI moiety (with an UV/vis absorption maximum at 578 nm in CH<sub>2</sub>Cl<sub>2</sub>). This steric demand of the individual chromophore as well as solvent polarity effects will strongly affect the interactions between the respective aromatic  $\pi$ -systems, and, as a consequence, the position of the equilibrium between  $\pi$ -stacked and nonstacked pinched cone conformation of the calix[4]arene unit will substantially be influenced (for a schematic representation of the conformational equilibrium see Figure 1).

The conformation-dependent photophysical properties of these bis-chromophoric systems are studied by means of UV/vis absorption, steady-state and time-resolved emission, femtosecond transient absorption spectroscopy, and spectrottemporal analysis of the femtosecond transient absorption data. The compounds studied as well as their syntheses and the structures of the related reference systems (without calix[4]arene substitution) are shown in Scheme 1. Thus, three compounds containing *one* PBI chromophore connected to a calix[4]arene unit (**oc**, **gc**, and **rc**), which are henceforth also referred to as “*monomers*”, three compounds containing *two* PBI moieties linked by one calix[4]arene unit (**o2c**, **g2c**, and **r2c**), which are referred to as “*dimers*”, and three reference PBI dyes containing no calix[4]arene units (**oref**, **gref**, and **rref**) are studied.

## Results and Discussion

**Synthesis and Structural Characterization.** The studied PBI–calix[4]arene arrays were synthesized according to Scheme 1. For this purpose, 1 equiv of 5,17-diamino-25,26,27,28-tetrakis(propoxy)-calix[4]arene was reacted with three different types (orange, green, and red) of perylene monoimide monoanhydrides to yield the 2-fold perylene-substituted calix[4]arene compounds **o2c**, **g2c**, and **r2c**. The imidization was carried out either in refluxing toluene/Et<sub>3</sub>N (for compound **r2c**) or in quinoline (at 165 °C for compound **o2c** and at 130 °C for compound **g2c**), using Zn(OAc)<sub>2</sub> as a catalyst. The monocalix[4]arene-substituted compounds **oc**, **gc**, and **rc** also shown in Scheme 1 were obtained under similar reaction conditions.<sup>24a,c,d</sup> All products were purified by column chromatography (SiO<sub>2</sub>) and were characterized by <sup>1</sup>H NMR spectroscopy, high resolution mass spectrometry, and elemental analysis.

Dark violet single crystals of compound **r2c** suitable for an X-ray analysis were obtained by slow crystallization from chloroform/methanol solution at room temperature. Hence, the crystals slightly differ in color compared to the red appearance in solution, which is most likely due to the packing of the PBI units. The molecule presents a pseudo 2-fold symmetry coincident with the calix[4]arene symmetry axis (see Figure 2). Two perylene units are oriented away from each other on opposite sides to the calix[4]arene, which is considerably distorted toward a pinched cone conformation. Neither of the perylene fragments exhibit a flat  $\pi$ -system but rather a propeller-like twisted conformation between their respective naphthalene half-units, as already observed for other bay-substituted PBIs.<sup>8</sup> The

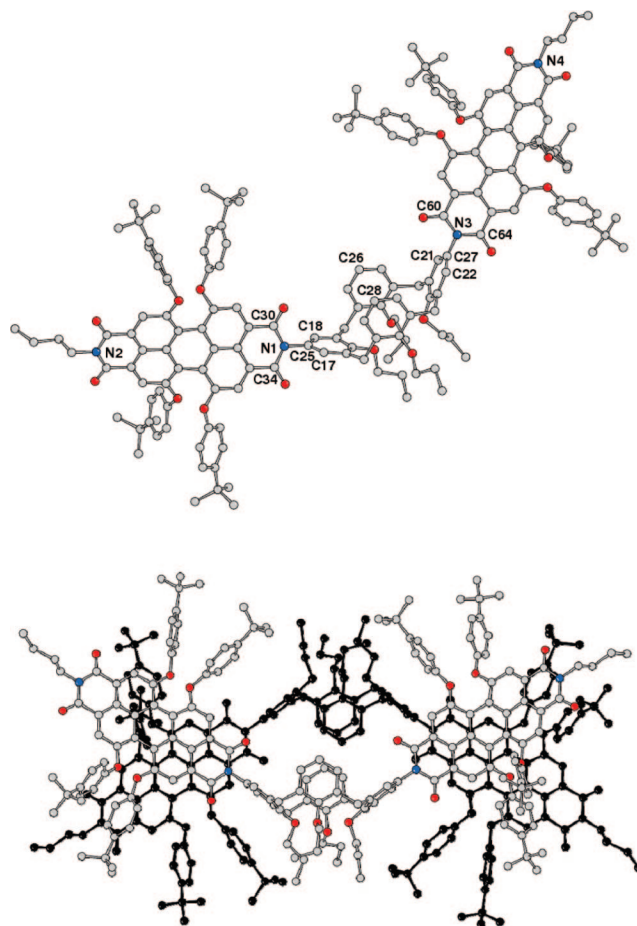


**Figure 2.** Top: Molecular structure of **r2c**. Bottom: View of the crystal packing of a pair of molecules related by a center of symmetry. Hydrogen atoms were omitted for clarity.

measured torsional angle of 29.4° is comparable with the value of 25° measured for other perylene derivative bearing tetraarylloxy-substituents at the bay-positions of the PBI core.<sup>25</sup> Noteworthy, the two PBI units are twisted in different directions to afford *P* and *M* helical configurations, respectively. This can be seen from the views of the molecular structure depicted in Figure 2 and Figures S5 and S6 in the Supporting Information (view of PBI units along the N bound to the calix[4]arene to the N bearing the butyl chain). For a visualization of the crystal packing, see Figure 2 (bottom), and for further details on the dihedral and torsion angles see Supporting Information.

**<sup>1</sup>H NMR Studies.** The <sup>1</sup>H NMR spectra in CDCl<sub>3</sub> of the monomeric compounds **oc**, **gc**, and **rc** as well as those of the dimeric compounds **o2c**, **g2c**, and **r2c** are sharp at room temperature. The observed signals correspond to the symmetry expected for the respective substitution pattern of the calix[4]arene moiety. A section of the spectra of compounds **oc** and **o2c** showing the signals of the Ar–CH<sub>2</sub>–Ar protons of the calix[4]arene moiety is exemplarily depicted in Figure 3 (for <sup>1</sup>H NMR data of the other compounds, see Figures S7 and S8 in the Supporting Information). Accordingly, *two* pairs of doublets for the protons of the methylene bridges are observed for compound **oc** (in agreement with *one* symmetry plane passing through the PBI-substituted phenolic ring of the calix[4]arene and through its nonsubstituted counterpart). For compound **o2c**, only *one* pair of doublets for the protons of the methylene bridges is found (in agreement with *two* symmetry planes present in the molecule). Likewise, for compounds **gc** and **rc**, two pairs of doublets for the protons of the methylene

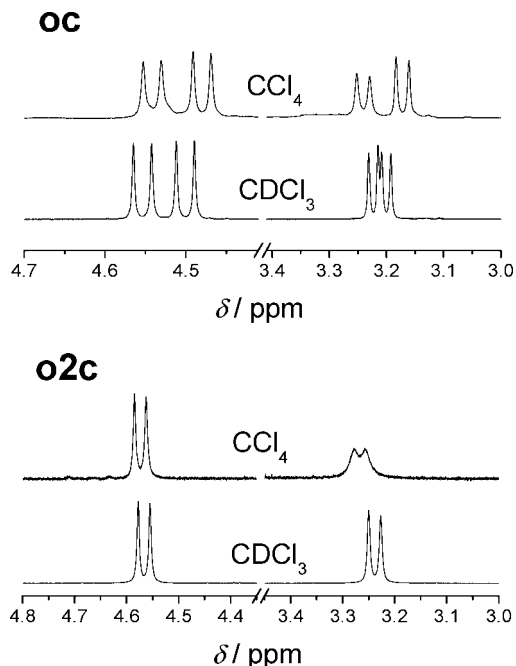


**Figure 3.** Sections of  $^1\text{H}$  NMR spectra (600 MHz, room temperature) showing the Ar-CH<sub>2</sub>-Ar protons of the respective calix[4]arene moiety in CCl<sub>4</sub> and CDCl<sub>3</sub> (indicated above in the individual spectrum) of compound **oc** (top) and compound **o2c** (bottom).

bridges are observed in the  $^1\text{H}$  NMR spectra, whereas, for compounds **g2c** and **r2c**, only one pair of doublets for the protons of the methylene bridges is present (see Figures S7 and S8 in the Supporting Information). Accordingly, for all monomeric and dimeric compounds, only one set of signals for the Ar-CH<sub>2</sub>-Ar protons of the calix[4]arene moiety is observed in CDCl<sub>3</sub>.

When changing to the less polar solvent CCl<sub>4</sub>, the signals of the Ar-CH<sub>2</sub>-Ar protons in the  $^1\text{H}$  NMR spectra of compound **oc** remain sharp at room temperature (see Figure 3). In contrast, the spectra of compound **o2c** in CCl<sub>4</sub> show a pronounced broadening of the doublet at higher field that is indicative for a dynamic process taking place on the NMR time scale. A similar behavior is also found in the spectra of compounds **g2c** and **r2c** in CCl<sub>4</sub> (see Figure S7 in the Supporting Information).

As discussed above, an equilibrium between the two possible pinched cone conformations of the calix[4]arene unit is expected for the dimeric compounds; with one conformation showing  $\pi$ -stacked arrangement of the PBI units, and the second conformation revealing nonstacked geometry as the PBI units point away from each other. Hence, the  $^1\text{H}$  NMR data should reveal the spectral features of both the  $\pi$ -stacked and the nonstacked pinched cone conformations, respectively, being in equilibrium with each other. The fact that only one set of sharp signals is detected in the  $^1\text{H}$  NMR spectra in CDCl<sub>3</sub> may be rationalized either by the fast interconversion between the two possible pinched cone conformations on the NMR time scale and that hence the observed spectra correspond to the weighted average of the signals, or the slow interconversion of the isomers on the NMR time scale, with the clear prevalence of one of the two pinched cone conformations. On the basis of our UV/vis absorption data (see below), however, the prevalence of the nonstacked pinched cone conformation can be safely assumed. Upon lowering the solvent polarity, the strength of  $\pi$ - $\pi$  interactions between PBI chromophores is known to increase substantially.<sup>8</sup> Accordingly, the equilibrium should be shifted toward the  $\pi$ -stacked pinched cone conformation. For such a

situation, line broadening can arise in the coalescence temperature range. The broadening of the  $^1\text{H}$  NMR signals of the Ar-CH<sub>2</sub>-Ar protons of **o2c** at room temperature in CCl<sub>4</sub> is accordingly attributed to such a dynamic process (see Figure 3).

To further elucidate this behavior, we have conducted variable temperature  $^1\text{H}$  NMR measurements in CCl<sub>4</sub> for all three compounds **o2c**, **g2c**, and **r2c**, respectively; for a section of the spectra showing the signals of the Ar-CH<sub>2</sub>-Ar protons of the respective calix[4]arene moiety, see Figure S9 in the Supporting Information.<sup>26</sup> Lowering of the temperature afforded coalescence at around 273 K for one set of the methylene protons of **o2c** and **g2c** as well as a broadening of the signal of the other methylene protons. For **r2c**, the temperature-dependent NMR spectra reveal several dynamical processes taking place in the given temperature range. These arise from complex motions of the phenoxy substituents between different conformational states and the interconversion of *M*- and *P*-atropoisomers of these in the bay area distorted dyes for which an energy barrier of around 60 kJ/mol has been determined recently.<sup>27</sup> Accordingly, the observed dynamic phenomena in the case of **r2c** can not be related to the equilibrium of the two calix[4]arene pinched cone conformations exclusively.

**Steady-State Optical Properties.** All compounds were characterized by means of UV/vis absorption and steady-state fluorescence emission spectroscopy in solvents of varying polarity employing methylcyclohexane (MCH,  $\epsilon_r = 2.0$ ), tetrachloromethane (CCl<sub>4</sub>,  $\epsilon_r = 2.2$ ), toluene ( $\epsilon_r = 2.4$ ), dichloromethane (CH<sub>2</sub>Cl<sub>2</sub>,  $\epsilon_r = 8.9$ ), and benzonitrile (PhCN,  $\epsilon_r = 25.9$ ). The related spectroscopic data are summarized in Table 1. Exemplarily, the UV/vis absorption spectra of compounds **o2c** and **g2c** obtained in various solvents are depicted in Figure 4 (top and bottom, respectively); the spectra of all other compounds are shown in the Supporting Information (Figure S11). The UV/vis absorption spectra are normalized for better comparison of the band shapes varying with changing solvent polarity.

The spectra of the *monomeric orange* compound **oc** show the characteristic vibronic UV/vis absorption pattern of the orange PBI chromophore in all solvents, thus being in good agreement with the spectral data obtained for the orange reference compound **oref** (for values of band maxima and molar extinction coefficients, see Table 1, and for spectra, see Figure S11 in the Supporting Information). A modest hypsochromic shift of the band maximum from 530 nm (in benzonitrile) to 517 nm (in MCH) is observed for compound **oc** as well as for **oref** (see Table 1). Furthermore, the values found for the ratio of the first and second absorption maxima (here denoted as (0,0)/(0,1)) range between 1.65 and 1.70 for compound **oc** and **oref** in all solvents (see Table 1), which thus indicates the presence of monomeric, nonaggregated dyes.

The absorption spectra of the *dimeric orange* compound **o2c** are depicted in Figure 4 (top). The spectrum in the most polar solvent benzonitrile (black line in Figure 4, top) shows the characteristic maxima of the orange PBI chromophore with bands at 530 and 493 nm very similar to those of the monomeric compound **oc** (see above), but reveals almost doubled values for the molar extinction coefficient of  $\epsilon(\text{PhCN}) = 162\,000\text{ M}^{-1}\text{ cm}^{-1}$  for the band at 530 nm. Hence, the absorption spectrum of compound **o2c** in benzonitrile consists of the absorption features of its constituent two orange PBI units, confirming an insignificant interaction between the chromophores in the ground-state in benzonitrile. Neither additional absorption bands emerged, nor did the absorption maxima shift to longer or shorter wavelengths. In contrast, when changing to solvents of

**TABLE 1: Steady-State Optical Properties in Various Solvents at Room Temperature<sup>a</sup>**

compd		MCH	CCl <sub>4</sub>	toluene	CH <sub>2</sub> Cl <sub>2</sub>	benzonitrile
<b>oc</b>	$\lambda_{\max}$ [ $\epsilon$ ]	517 [96400] 480 [56500]	523 [94800] 487 [56600]	527 [86400] 491 [52500]	526 [91600] 489 [55200]	530 [88900] 493 [53500]
	$\lambda_{\max}$ [ $\Phi_{\text{FI}}$ ] (0,0)/(0,1) <sup>b</sup>	520, 558 [0.01] 1.70	526, 566 [0.02] 1.68	534, 576 [0.02] 1.65	535, 573 [0.03] 1.65	537, 579 [0.02] 1.66
<b>o2c</b>	$\lambda_{\max}$ [ $\epsilon$ ]	522 [67100] <sup>c</sup> 486 [106500]	525 [89700] 489 [95800]	527 [114600] 490 [90700]	526 [164200] 490 [106700]	530 [162000] 493 [103400]
	$\lambda_{\max}$ [ $\Phi_{\text{FI}}$ ] (0,0)/(0,1) <sup>b</sup>	522, 562 [ $<0.01$ ] 0.63	527, 569 [ $<0.01$ ] 0.94	532, 574 [ $<0.01$ ] 1.26	536, 577 [0.03] 1.54	538, 580 [0.03] 1.57
<b>oref</b>	$\lambda_{\max}$ [ $\epsilon$ ]	517 [93700] 480 [55200]	523 [96800] 487 [57500]	527 [92200] 490 [55800]	527 [93600] 490 [56000]	531 [91100] 494 [54500]
	$\lambda_{\max}$ [ $\Phi_{\text{FI}}$ ] (0,0)/(0,1) <sup>b</sup>	521, 561 [ $\sim 1.00$ ] <sup>d</sup> 1.70	527, 569 [ $\sim 1.00$ ] <sup>d</sup> 1.68	535, 579 [ $\sim 1.00$ ] <sup>d</sup> 1.65	534, 576 [0.99] 1.67	540, 583 [ $\sim 1.00$ ] <sup>d</sup> 1.67
<b>gc</b>	$\lambda_{\max}$ [ $\epsilon$ ]	664 [44900]	680 [43300]	686 [43100]	701 [47300]	705 [45600]
	$\lambda_{\max}$ [ $\Phi_{\text{FI}}$ ]	685 [0.41]	704 [0.37]	721 [0.29]	742 [0.19]	748 [0.17]
<b>g2c</b>	$\lambda_{\max}$ [ $\epsilon$ ]	709 [30700] <sup>c</sup> 657 [33300]	680 [67600]	686 [66500]	706 [92400]	706 [83800]
	$\lambda_{\max}$ [ $\Phi_{\text{FI}}$ ]	684, 756 [ $<0.01$ ]	706 [0.12]	723 [0.27]	744 [0.22]	750 [0.17]
<b>grf</b>	$\lambda_{\max}$ [ $\epsilon$ ]	669 [44700]	686 [44100]	692 [46100]	709 [43000]	710 [45200]
	$\lambda_{\max}$ [ $\Phi_{\text{FI}}$ ]	691 [0.39]	708 [0.34]	727 [0.24]	748 [0.19]	753 [0.18]
<b>rc</b>	$\lambda_{\max}$ [ $\epsilon$ ]	564 [45600]	572 [47900]	573 [47300]	578 [47400]	580 [43800]
	$\lambda_{\max}$ [ $\Phi_{\text{FI}}$ ]	588 [ $\sim 1.00$ ] <sup>d</sup>	596 [0.99]	600 [ $\sim 1.00$ ] <sup>d</sup>	608 [0.80]	614 [0.81]
<b>r2c</b>	$\lambda_{\max}$ [ $\epsilon$ ]	571 [72200] 534 [49800]	573 [90100]	573 [92800]	580 [92200]	581 [88000]
	$\lambda_{\max}$ [ $\Phi_{\text{FI}}$ ]	588 [0.29]	596 [ $\sim 1.00$ ] <sup>d</sup>	600 [ $\sim 1.00$ ] <sup>d</sup>	612 [0.79]	615 [0.82]
<b>rref</b>	$\lambda_{\max}$ [ $\epsilon$ ]	567 [47400]	578 [50600]	579 [49800]	582 [49700]	586 [46500]
	$\lambda_{\max}$ [ $\Phi_{\text{FI}}$ ]	593 [0.96]	604 [0.96]	608 [0.97]	615 [0.99]	620 [0.95]

<sup>a</sup> Values for  $\epsilon$  are given in ( $\text{M}^{-1}\text{cm}^{-1}$ ) and values of  $\lambda_{\max}$  in (nm). Optical density (OD) of the solution  $\sim 1$ . The shape of the spectra did not change upon dilution. <sup>b</sup> Denoting the ratio of first and second absorption maxima. <sup>c</sup> Precipitation from solution after ca. 30 min. <sup>d</sup>  $\Phi_{\text{FI}} \pm 0.02$ .

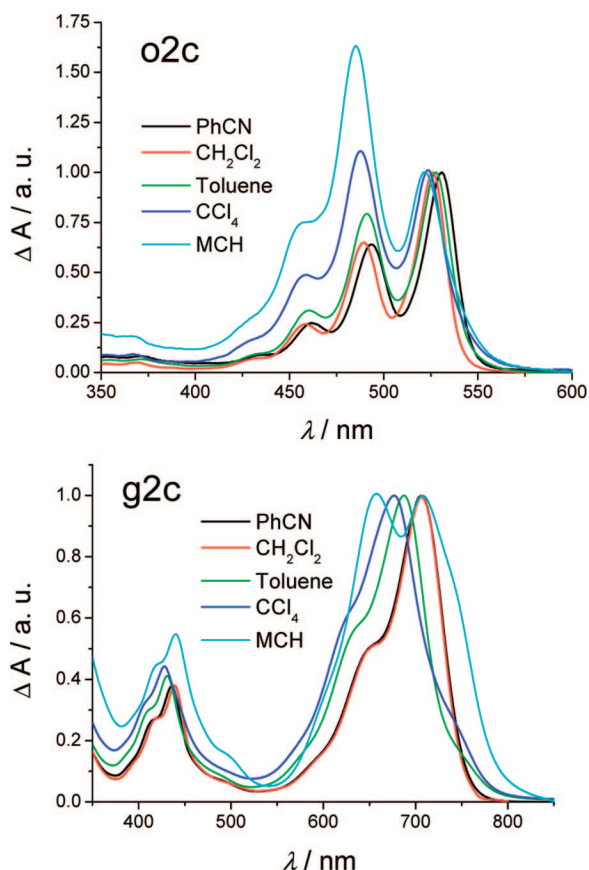


**Figure 4.** Normalized UV/vis absorption spectra in benzonitrile (PhCN, black line), CH<sub>2</sub>Cl<sub>2</sub> (red line), toluene (green line), CCl<sub>4</sub> (blue line), and MCH (cyan line) of compound **o2c** (top) and of compound **g2c** (bottom).

lower polarity the spectral features of the dimeric compound **o2c** differ significantly from those of the monomer **oc**. Thus,

the absorbance around 490 nm shows a dramatic increase relative to that around 525 nm for all solvents (for the respective changes in the molar extinction coefficients, see Table 1). Accordingly, values for the (0,0)/(0,1) ratio are found to be 1.54 in CH<sub>2</sub>Cl<sub>2</sub>, 1.26 in toluene, 0.94 in CCl<sub>4</sub>, and 0.63 in MCH.

These spectral features are typical for  $\pi$ -stacked PBI chromophores in a sandwich-type arrangement, where the transition dipole moments of the dye units are cofacially arranged.<sup>28–30</sup> For such an arrangement, the strong excitonic coupling results in a hypsochromically shifted main absorption band (called the H-band) compared to nonaggregated PBI dye units. As illustrated in Figure 1, the two possible pinched cone conformations of the calix[4]arene unit are characterized by one conformation showing  $\pi$ -stacked arrangement of the PBI units and the second conformation revealing nonstacked geometry as the PBI units point away from each other. Hence, the UV/vis absorption curves (shown in Figure 4, top) reveal the superimposed spectral features of both the  $\pi$ -stacked and nonstacked pinched cone conformations, which are in equilibrium with each other. For the first conformation, the two PBI chromophores are  $\pi$ -stacked in a parallel sandwich-type geometry with almost no longitudinal offset. A hypsochromic spectral shift is expected for such H-type aggregates as observed in the low polarity solvents (see Figure 4, top).<sup>28,29</sup> For the other pinched cone conformation with nonstacked arrangement of the PBI chromophores, we may expect almost unchanged spectra compared to those of the orange monomers **oc** and **oref** as a result of the almost orthogonal orientation of the transition dipole moments of the two dye units and the significant distance between the centers of the chromophores. Indeed, these spectral features of nonaggregated chromophores are observed for the more polar solvents CH<sub>2</sub>Cl<sub>2</sub> and benzonitrile. Accordingly, these solvent-dependent spectra reveal a shift of the equilibrium between the two pinched cone conformations upon lowering the solvent polarity toward the  $\pi$ -stacked conformation, thus

enhancing the spectral features of the  $\pi$ -stacked pinched cone conformation (see Figure 4, top), whereas, for polar solvents, the nonstacked conformation clearly dominates the spectra.

Likewise, as observed for the orange compounds **oc** and **oref**, the spectra of the *green monomeric* compounds **gc** and **gref** also exhibit the characteristic UV/vis absorption maxima of the green PBI chromophore in all solvents (see Table 1 and Supporting Information). Thus, no significant changes in the general band shapes are observed upon lowering the solvent polarity. The positive solvatochromism from 664 nm in MCH to 705 nm in benzonitrile for compound **gc** and from 669 nm in MCH to 710 nm in benzonitrile in compound **gref** is in accordance with the pronounced charge transfer character of the  $S_0 \rightarrow S_1$  transition for the green chromophore.<sup>31</sup> The related spectra of the *green dimeric* compound **g2c** are shown in Figure 4, bottom. No indication for the formation of a  $\pi$ -stacked pinched cone conformation of the calix[4]arene unit in an H-type aggregation arrangement is observed for the spectra in the polar solvents benzonitrile,  $\text{CH}_2\text{Cl}_2$ , and toluene. In contrast, the spectra of **g2c** in  $\text{CCl}_4$  reveal a loss of fine-structure and broadening of the band, and for the spectra in MCH, a split band with two maxima at 657 and 709 nm, respectively, is observed. These findings again confirm the presence of equilibrium between the two possible pinched cone conformations in compound **g2c**, which is shifted toward the  $\pi$ -stacked conformation in solvents of very low polarity.

For all three *red* compounds, **rc**, **rref**, and **r2c**, a modest hypsochromic shift of the UV/vis absorption maxima upon lowering the solvent polarity from benzonitrile to MCH is observed (see Table 1 and Figure S11 in the Supporting Information). No significant changes in the band shapes are found, except a small band enhancement at 534 nm for *red dimeric* compound **r2c** in MCH that might indicate a small amount of  $\pi$ -stacked pinched cone conformation.

**Temperature-Dependent UV/Vis Absorption Spectra.** To exclude the presence of *intermolecular* PBI aggregates at the given concentrations, temperature-dependent UV/vis absorption measurements have been carried out that are depicted in Figure 5 and in Figure S12 and S13 in the Supporting Information. For entropic reasons, *intermolecular* aggregates would dissociate into the respective monomer species at higher temperatures,<sup>32</sup> and the absorption spectra at higher temperatures would thus reveal the spectral features of the monomer species. In contrast, the interactions within *intramolecular* aggregates would not be changed with respect to the increasing temperature and thus the UV/vis absorption spectra upon heating of the solution would not be influenced substantially. Accordingly, UV/vis absorption spectra of the dimeric compounds **o2c**, **g2c**, and **r2c** in  $\text{CCl}_4$  as well as those of their related monomers **oc**, **gc**, and **rc** and of the PBI reference compounds **oref**, **gref**, and **rref** were recorded for dilute solutions as a function of the temperature in the range from 20 to 70 °C, with heating steps of 10 °C. For the sake of illustration, the spectra of compound **oc** and **o2c** are shown in Figure 5, all other spectra are depicted in Figure S12 and S13 in the Supporting Information.<sup>33</sup> The UV/vis absorption spectra of **o2c** and **g2c** in  $\text{CCl}_4$  show that both compounds remain  $\pi$ -stacked, even at elevated temperature and very low concentrations of ca.  $5.0 \times 10^{-6}$  M. This  $\pi$ -stacking can only be attributed to an *intramolecular* aggregation of the PBI chromophores because an *intermolecular* aggregate would show strong temperature and concentration dependence in the UV/vis spectra.<sup>10c,32,34</sup>

**Steady-State Fluorescence Emission Spectra.** All compounds have been investigated by steady-state fluorescence spectroscopy, and the values obtained for quantum yields and

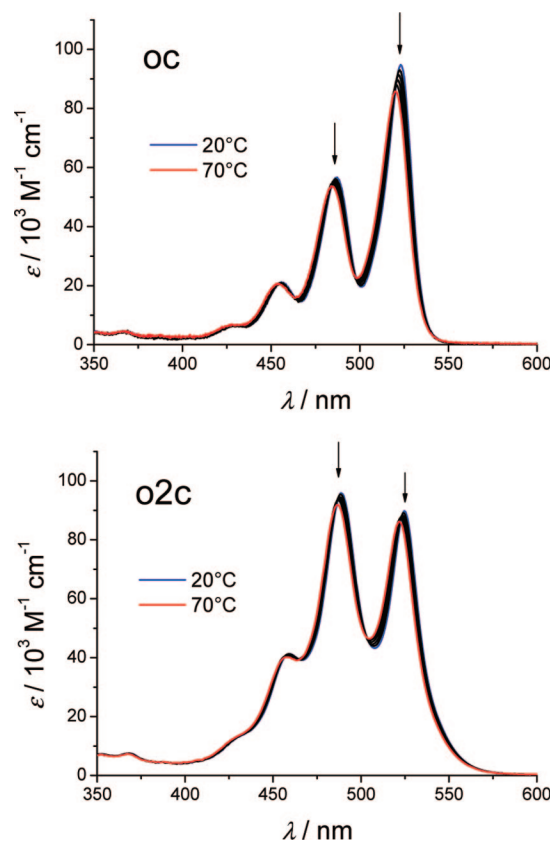


**Figure 5.** UV/vis absorption spectra at variable temperatures in  $\text{CCl}_4$  of compound **oc** (top,  $c = 4.56 \times 10^{-6}$  M) and of compound **o2c** (bottom,  $c = 5.83 \times 10^{-6}$  M), concentrations given at 20 °C. Arrows indicate trends upon rising temperature. Spectra are corrected for density changes due to rising temperature.

band maxima in the various solvents are summarized in Table 1. The emission spectra of the *orange* monomeric compound **oc** and those of the dimeric compound **o2c** are depicted in Figure 6; for all other fluorescence spectra, see Figure S14 in the Supporting Information. The emission spectra of compound **oc** show the characteristic vibronic progressions of a nonaggregated orange PBI, being in good agreement with those of the orange reference compound **oref**. They are showing a hypsochromic shift of 17 nm from 537 nm in benzonitrile to 520 nm in MCH for compound **oc** due to solvatochromic effects similar to those already observed in the UV/vis absorption spectra (see Table 1). In contrast, the spectra of the dimeric compound **o2c** in Figure 6 reveal an additional broad, red-shifted emission band at around 650 nm for all solvents, accompanied by a hypsochromic shift of the band maximum of 16 nm when changing from benzonitrile to MCH (see Table 1). The broad emission feature is increasing in intensity upon lowering the solvent polarity and becomes most pronounced in MCH. Furthermore, the values for the fluorescence quantum yields for the dimeric compound **o2c** decrease in solvents of lower polarity, whereas, for the respective monomeric compound **oc**, comparably higher values are found (see Table 1).<sup>36</sup> The observed broad spectral features can be attributed to an “excimer-type” emission resulting from  $\pi$ -stacked PBI chromophores.<sup>32</sup> Hence, also for the steady-state fluorescence spectra, a solvent-polarity dependence is observed, indicating the presence of an equilibrium between the two pinched cone calix[4]arene conformations. The fluorescence quantum yields (see Table 1) also support this trend, as solvent polarity-dependent fluorescence quenching is observed, being typical for  $\pi$ -stacked sandwich aggregates of H-type arrangement.

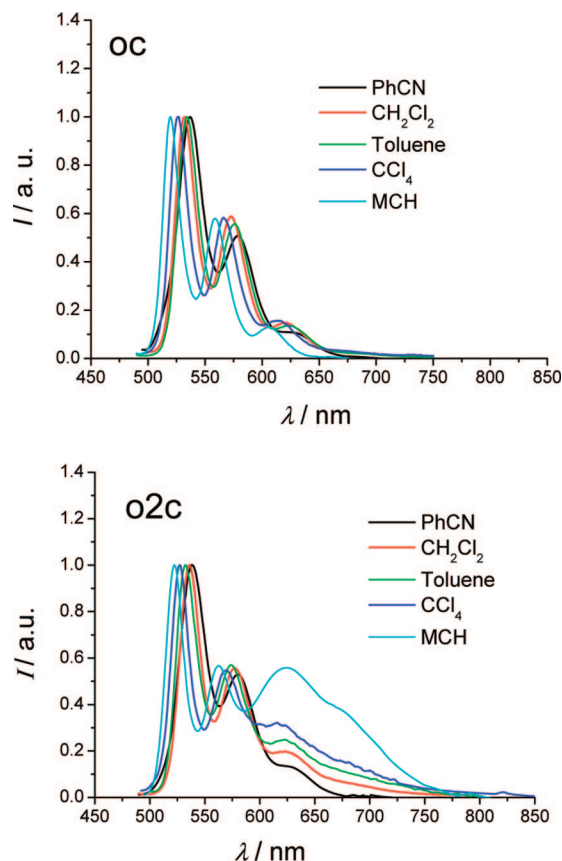


**Figure 6.** Normalized steady-state fluorescence spectra in benzonitrile (PhCN, black line),  $\text{CH}_2\text{Cl}_2$  (red line), toluene (green line),  $\text{CCl}_4$  (blue line), and MCH (cyan line) under dilute conditions (OD of the respective solution  $< 0.05$ ) of compound **oc** (top) and of compound **o2c** (bottom).

The emission spectra of both the monomeric and dimeric green compounds **gc** and **g2c** show the characteristic fluorescence spectral features of a monomeric green PBI chromophore in benzonitrile,  $\text{CH}_2\text{Cl}_2$ , toluene, and  $\text{CCl}_4$  (see Table 1), being in reasonable agreement with the data for the green reference compound **gref**. Furthermore, hypsochromic shifts of 63 and 66 nm are found for compounds **gc** and **g2c** from benzonitrile to MCH, respectively, as a result of the pronounced solvatochromic behavior of this charge transfer transition (see Table 1). Only in MCH do the spectra of compound **g2c** reveal a distinct additional broad emission band at around 756 nm. Furthermore, the fluorescence quantum yields determined for the compounds **g2c**, **gc**, and **gref** (given in Table 1) show very similar values in benzonitrile ( $\Phi_{\text{fl}} = 0.17\text{--}0.18$ ),  $\text{CH}_2\text{Cl}_2$  ( $\Phi_{\text{fl}} = 0.19\text{--}0.22$ ), and in toluene ( $\Phi_{\text{fl}} = 0.24\text{--}0.27$ ) but very different values in  $\text{CCl}_4$  and MCH. Thus, a strong fluorescence quenching is observed for compound **g2c** in  $\text{CCl}_4$  and MCH ( $\Phi_{\text{fl}} = 0.12$  in  $\text{CCl}_4$  and  $\Phi_{\text{fl}} < 0.01$  in MCH) compared with those for the respective monomeric compound **gc** ( $\Phi_{\text{fl}} = 0.37$  in  $\text{CCl}_4$  and  $\Phi_{\text{fl}} = 0.41$  in MCH) and to those of the green reference compound **gref** without calix[4]arene substitution ( $\Phi_{\text{fl}} = 0.34$  in  $\text{CCl}_4$  and  $\Phi_{\text{fl}} = 0.39$  in MCH). These findings corroborate the presence of an equilibrium between the two possible pinched cone conformations of the calix[4]arene unit for compound **g2c** in MCH, and these results thus closely reflect the observations made for the UV/vis absorption spectra of **g2c**. The  $\pi$ -stacking in the green system is, however, only observed for the spectra in MCH and to a lesser extent in  $\text{CCl}_4$  which is most likely due to the steric hindrance of the substituents in

the bay positions of the PBI chromophore that destabilize the close van der Waals contact between the two  $\pi$ -surfaces.

Almost no changes in the emission spectra as a function of solvent polarity are observed for the red monomeric and dimeric compounds **rc** and **r2c**. Only for the lowest polarity solvent MCH is a slightly enhanced absorbance at 534 nm found for compound **r2c**. Concomitantly, equally high fluorescence quantum yields  $\Phi_{\text{fl}} > 0.80$  are found for **r2c** and **rc** in all solvents with the exception of MCH. In this particular solvent, a strong fluorescence quenching is observed for compound **r2c** ( $\Phi_{\text{fl}} = 0.29$ ), revealing the formation of the  $\pi$ -stacked conformer in the excited state.

**Molecular Modeling Studies.** To further elaborate these findings on a theoretical level, molecular modeling studies were performed at the force-field level (Amber 9,<sup>37</sup> Generalized Amber Force Field (GAFF)<sup>38</sup> using AM1BCC partial charges;<sup>39</sup> for details see Supporting Information) to determine the relative stabilities of the  $\pi$ -stacked and non- $\pi$ -stacked conformers of the least sterically hindered **o2c** dimer and the most sterically hindered **r2c** dimer in polar and nonpolar environments. For the calculations in a polar environment, the acetonitrile model of Grabuleda et al. was utilized,<sup>40</sup> whereas the limiting case of a nonpolar environment was represented by vacuum. The resulting potentials of mean force (PMFs; see Figures 7 and 8) of both molecules bear two local minima corresponding to  $\pi$ -stacked conformations of the molecules and a third significantly wider well corresponding to the non- $\pi$ -stacked conformations. The first  $\pi$ -stacked conformation is characterized by a crossing of the N–N axes of the two chromophores, while the second exhibits parallel N–N axes. In non- $\pi$ -stacked conformations, the chromophores are far away from each other (for structures, see Figure S15 in the Supporting Information). The PMF for **o2c** indicates that in vacuo  $\pi$ -stacked conformations are lower in free energy than non- $\pi$ -stacked conformations (see Figure 7). In  $\text{CH}_3\text{CN}$ , however, the relative stabilities are reversed, with non- $\pi$ -stacked conformations lying lower on the PMF than  $\pi$ -stacked conformations. These findings are in excellent agreement with the results obtained by UV/vis absorption and fluorescence spectroscopy, as discussed in the previous section. The locations of free energy wells of  $\pi$ -stacked conformations and their actual geometries observed from molecular dynamics snapshots do not vary significantly between simulations in vacuo and  $\text{CH}_3\text{CN}$ , while the free energy well corresponding to non- $\pi$ -stacked conformations is shifted to a larger interchromophoric distance in vacuo.

The PMF for **r2c** in  $\text{CH}_3\text{CN}$  (see Figure 8) indicates that non- $\pi$ -stacked conformations are lower in free energy than  $\pi$ -stacked conformations, mirroring the PMF for **o2c** in  $\text{CH}_3\text{CN}$ , which again resembles very nicely the conclusions drawn from the experimentally obtained UV/vis absorption and fluorescence emission data. In vacuo, the lowest free energy well contains partially  $\pi$ -stacked conformations with bulky *tert*-butylphenoxy substituents caught in between the two PBI units, leading to a greater interchromophoric separation ( $\sim 7$  Å). All conformations with direct  $\pi$ -stacking between two red PBI chromophores ( $d < 5$  Å) are significantly higher in energy. Hence, only a weak excitonic coupling between the red PBI chromophores is expected for **r2c**, even in low polarity solvents.

Interchromophoric distance expectation values  $\langle d_i \rangle$  were calculated for each free energy well by taking the product of probability and distance at each PMF point in the well and summing over each well. Expectation values of relative free energy  $\langle \Delta G_{ij} \rangle$  were calculated as the difference between the PMF expectation values in each well. The results are summarized in

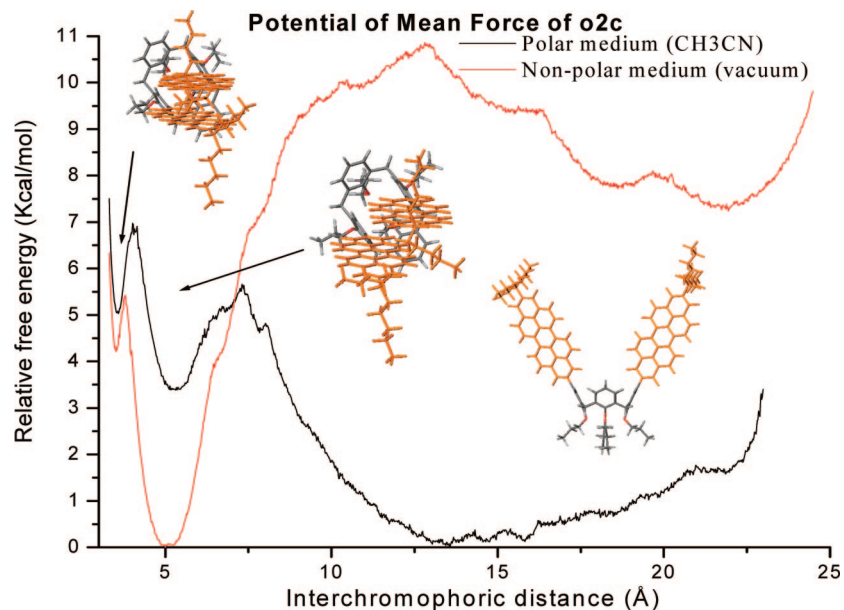


**Figure 7.** Free energy as a function of **o2c** interchromophoric distance in explicit acetonitrile solution (black line, representative for polar solvents) and *in vacuo* (red line, representative for nonpolar solvents) derived from probability distributions extracted from molecular dynamics simulations. Structures found in each free energy well are shown as insets and include  $\pi$ -stacked crossed conformations between 3 and 4 Å (left),  $\pi$ -stacked parallel conformations between 4 and 6 Å (middle), and the non- $\pi$ -stacked conformations found over the range of approximately 10 to 25 Å (right).

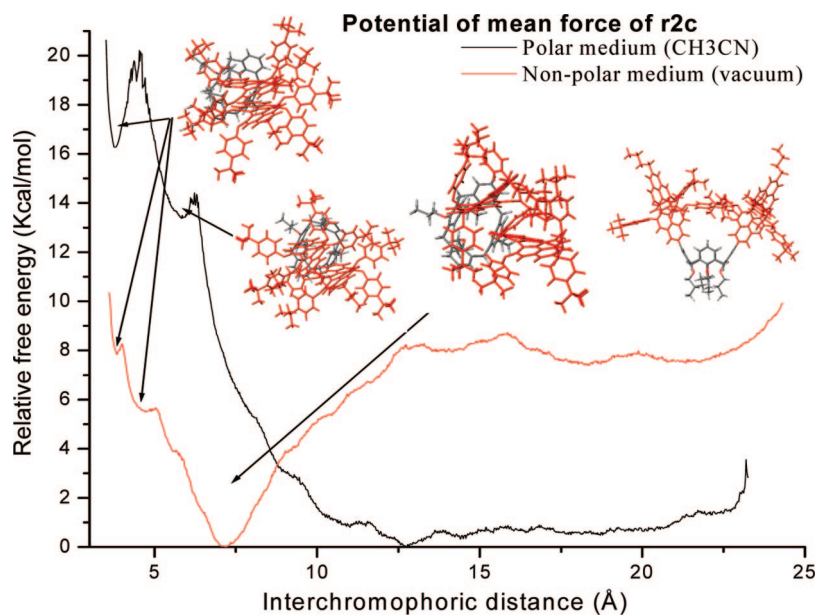


**Figure 8.** Free energy as a function of **r2c** interchromophoric distance in explicit acetonitrile solution (black line, representative for polar solvents) and *in vacuo* (red line, representative for nonpolar solvents) derived from probability distributions extracted from molecular dynamics simulations. Structures found in each free energy well are shown as insets and include  $\pi$ -stacked crossed conformations between 3 and 5 Å (far left),  $\pi$ -stacked parallel conformations between 5 and 6 Å (inner left), sterically hindered partially  $\pi$ -stacked conformations between approximately 6 and 9 Å (inner right) and non- $\pi$ -stacked conformations found over the range of approximately 10 to 25 Å (far right).

Table 2, and they are clearly consistent with the respective stability of the two dimer compounds in nonpolar versus polar media as described above.

INDO/SCI<sup>41</sup> excited-state calculations were performed on crossed  $\pi$ -stacked and non- $\pi$ -stacked geometries of **o2c** to enable the comparison of their spectroscopic features. The geometries were obtained by averaging atomic coordinates of molecular dynamics snapshots found in each free energy well followed by minimization to take the system to the nearest local minima. The simulated absorption spectrum of **o2c** in the  $\pi$ -stacked conformation exhibits a hypsochromic shift by  $\sim 0.17$  eV of the main absorption band relative to the non- $\pi$ -stacked

one, as expected for a H-type aggregate (see Figure 9). This is again in good agreement with the experimentally obtained UV/vis data where a shift of the absorption band from 520 (2.38 eV) to 486 nm (2.55 eV) is observed upon  $\pi$ -stacking for **o2c** in nonpolar solvents. Thus, as predicted from the quantum chemical calculations, the  $\pi$ -stacked conformation yields a vertical excitation energy that is blue-shifted by about 1 vibrational quantum with respect to the nonstacked conformation. Transition density distributions calculated for the optical transitions I and III in the spectrum of the  $\pi$ -stacked form are shown as insets in Figure 9 and correspond to out-of-phase (J-band) and in-phase (H-band) combinations of the molecular

**TABLE 2: Free Energy Well Interchromophoric Separation Expectation Values  $\langle d_i \rangle$  and Relative Free Energies of Neighboring Wells Measured as the Difference in PMF Expectation Values  $\langle \Delta G_{ij} \rangle$  Between Wells**

	<b>o2c</b> in CH <sub>3</sub> CN	<b>o2c</b> in vacuo	<b>r2c</b> in CH <sub>3</sub> CN	<b>r2c</b> in vacuo
$\langle d_1 \rangle$ (Å)	3.6	3.6	3.8	4.7
conformation	$\pi$ -stacked crossed	$\pi$ -stacked crossed	$\pi$ -stacked crossed	$\pi$ -stacked crossed
$\langle \Delta G_{12} \rangle$ (kcal/mol)	-1.7	-4.3	-2.9	-5.3
$\langle d_2 \rangle$ (Å)	5.4	5.1	5.8	7.2
conformation	$\pi$ -stacked parallel	$\pi$ -stacked parallel	$\pi$ -stacked parallel	partially $\pi$ -stacked
$\langle \Delta G_{23} \rangle$ (kcal/mol)	-3.2	7.4	-13.1	7.3
$\langle d_3 \rangle$ (Å)	15.0	20.7	15.7	19.7
conformation	nonstacked	nonstacked	nonstacked	nonstacked

transition dipoles, respectively. Optical transition II has clear charge-transfer character with the majority of electron and hole excited-state wave function density lying on opposite PBI chromophores. As a result of geometric relaxation in the excited state, we expect the emission to take place from an excimer-like species, i.e., an electronic transition intermediate between excitations I and II above, which is consistent with the broad, strongly red-shifted solvent-dependent fluorescence band at  $\sim 650$  nm and the low emission quantum yield in polar solvents.

The same INDO/SCI calculations have been performed for two representative structures of the nonstacked and partially  $\pi$ -stacked conformations of **r2c**. The results (not shown) indicate a very limited ( $<0.1$  eV) blue shift in going from the former to the latter, consistent with a small excitonic coupling between the two sterically hindered PBI cores in **r2c**.

As substantiated by the molecular modeling study, the steady-state spectroscopy shows that a  $\pi$ -stacked conformer is present for the dimers in nonpolar solvents and that the **o2c** dimer is

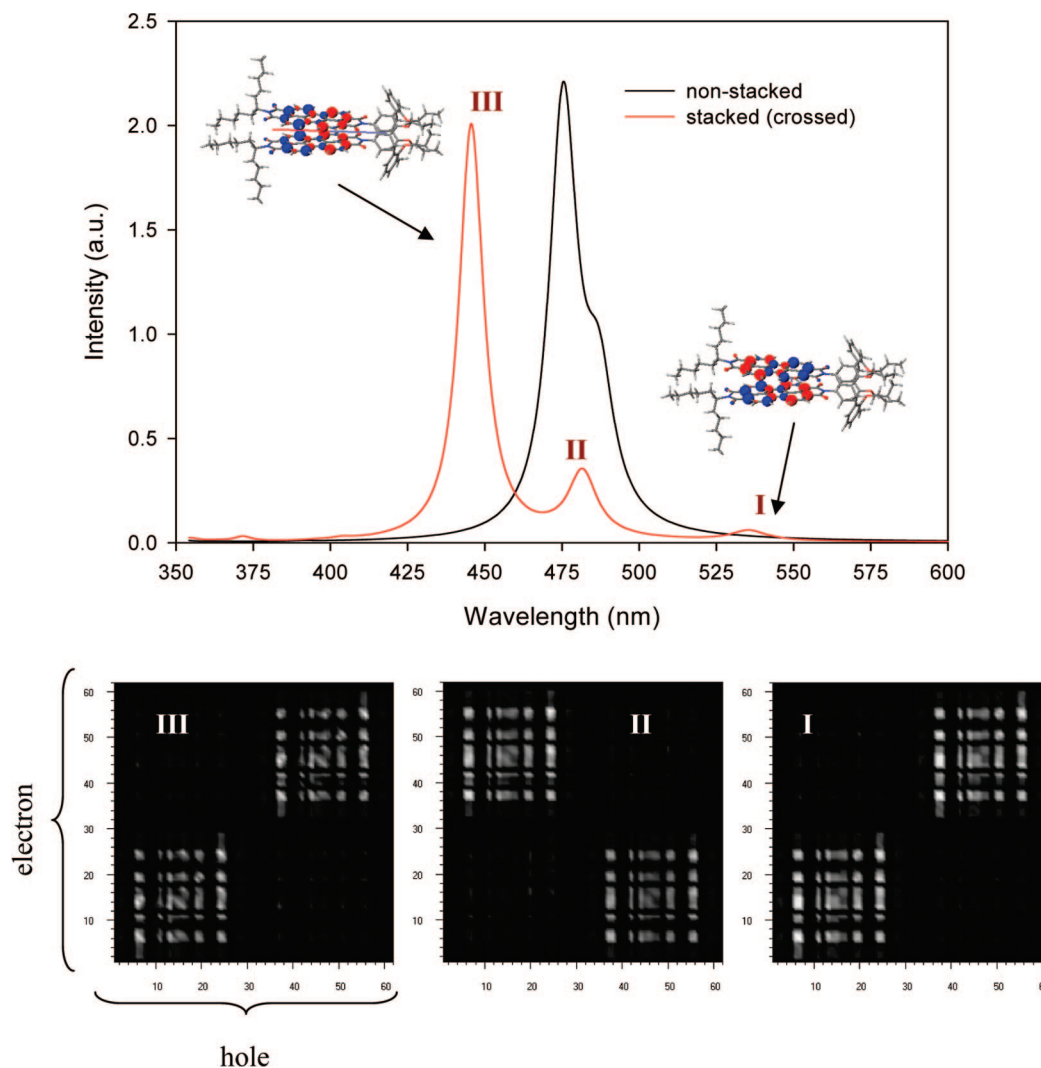


**Figure 9.** (Top) Simulated absorption spectra of the orange dye in the  $\pi$ -stacked and nonstacked conformations (INDO/SCI excited-state calculations on the basis of the force field geometries; Lorentzian functions with 0.06 eV half-width have been used to convolute the spectra). The transition density distributions calculated for the optical transitions I and III are shown as insets; these correspond to out-of-phase and in-phase combinations of the molecular transition dipoles. (Bottom) Hole–electron excited-state wave functions vs atom index for the states labeled I, II, and III on the spectrum of the stacked conformation. Note the charge-transfer character of state II (with predominant off-diagonal contributions, i.e., hole and electron on different PBI units).

TABLE 3: Fluorescence Lifetimes in Various Solvents<sup>a</sup>

compd	$\tau$ (ns) MCH	$\tau$ (ns) CCl <sub>4</sub>	$\tau$ (ns) toluene	$\tau$ (ns) CH <sub>2</sub> Cl <sub>2</sub>	$\tau$ (ns) benzonitrile
oref <sup>b</sup>	4.2	4.1	4.0	4.9	3.9
oc	— <sup>c</sup>	— <sup>c</sup>	— <sup>c</sup>	— <sup>c</sup>	— <sup>c</sup>
o2c <sup>d</sup>	—	0.15	0.15	0.14	0.16
gref <sup>e,f</sup>	5.9	5.6	4.3	3.1	2.5
gc <sup>e</sup>	6.1	5.6	4.4	3.3	2.7
g2c <sup>e</sup>	— <sup>d</sup>	— <sup>g</sup>	4.4	3.3	2.8
rref <sup>h</sup>	6.3	6.9	6.1	6.9	6.3
rc	5.9	6.3	6.3	5.6	4.7
r2c	7.4	6.3	5.8	5.7	4.9

<sup>a</sup> All spectra recorded at room temperature. <sup>b</sup> Data are in good agreement with the literature value of  $\tau = 3.7$  ns for a similar orange reference in CHCl<sub>3</sub>; see refs 8 and 12a. <sup>c</sup> Values could not be determined, as the signal falls into the time response of the instrument of ca. 150 ps. <sup>d</sup> In MCH precipitation was observed during the time frame of the experiment. In other solvents, a second long-lived emission was observed that is attributed to a strongly fluorescent impurity/decomposition product containing the orange PBI chromophore (values given in ns with respective amplitudes in brackets): 2.6 (25%) in CCl<sub>4</sub>, 2.9 (2%) in toluene, 2.9 (2%) in CH<sub>2</sub>Cl<sub>2</sub>, and 3.0 (0.5%) in benzonitrile. <sup>e</sup> Note that, for all lifetimes determined for compounds **g2c**, **gc**, and **gref**, biexponential decays were observed. Accordingly, additional small components are found which are considered to be inherent to the green PBI chromophore itself (values given in ns with the respective amplitudes in brackets): For compound **gref**: 0.4 (10%) in MCH, 0.6 (12%) in CCl<sub>4</sub>, 0.7 (5%) in toluene, 0.4 (8%) in CH<sub>2</sub>Cl<sub>2</sub>, and 0.3 (30%) in benzonitrile. For compound **gc**: 0.7 (12%) in MCH, 0.3 (30%) in CCl<sub>4</sub>, 0.5 (20%) in toluene, 0.4 (15%) in CH<sub>2</sub>Cl<sub>2</sub>, and 0.2 (30%) in benzonitrile. For compound **g2c**: 0.5 (15%) in toluene, 0.8 (8%) in CH<sub>2</sub>Cl<sub>2</sub>, and 0.6 (8%) in benzonitrile. <sup>f</sup> Data are in good agreement with the literature value of  $\tau = 4.5$  ns for a similar green reference in toluene; see ref 8. <sup>g</sup> Degradation of the sample during the time frame of experiment. <sup>h</sup> Data are in good agreement with literature values in CHCl<sub>3</sub> of  $\tau = 6.5$  ns in ref 11 and of  $\tau = 7.4$  ns in ref 12b.

most prone to this stacking. In order to probe the excited-state behavior of these dimers, various types of time-resolved spectroscopy were employed as discussed in the following section.

**Time-Resolved Emission Spectroscopy.** The fluorescence lifetimes of all compounds have been determined, and the respective data are summarized in Table 3. For the orange reference compound **oref**, fluorescence lifetimes between 3.9 and 4.9 ns have been determined, showing no dependence on solvent polarity. For both compounds **oc** and **o2c**, a drastically shortened fluorescence lifetime compared to the value of the orange reference compound **oref** is found, which has been attributed in our earlier work on **oc** to a very efficient photoinduced electron transfer process ( $k_{CT} = 3.1 \times 10^{10} \text{ s}^{-1}$  in CH<sub>2</sub>Cl<sub>2</sub>) between the electron-poor orange PBI unit and the electron-rich calix[4]arene substituent.<sup>24c,36</sup> The observed lifetimes for **oc** are thus reduced to values lower than the system response of approximately 150 ps. For compound **o2c**, lifetime values in the range of the system response of about 150 ps are measured. For the green and red systems **g2c** and **r2c**, no significant variations due to photoinduced electron transfer or excimer formation can be extracted from the data, as the measured lifetime values are in good accordance with the emission of the non- $\pi$ -stacked reference chromophores (see Table 3 and further details in the Supporting Information).<sup>43</sup>

**Femtosecond Transient Absorption Spectroscopy.** The femtosecond transient absorption spectra of compounds **oc** and **o2c** in CCl<sub>4</sub> are depicted in Figure 10. For compound **oc** upon photoexcitation at 530 nm in CCl<sub>4</sub>, an intense bleaching is observed at 530 and 485 nm ( $S_0 \rightarrow S_1$  transitions of the orange PBI chromophore<sup>24c,44</sup>) as well as an intense negative signal at

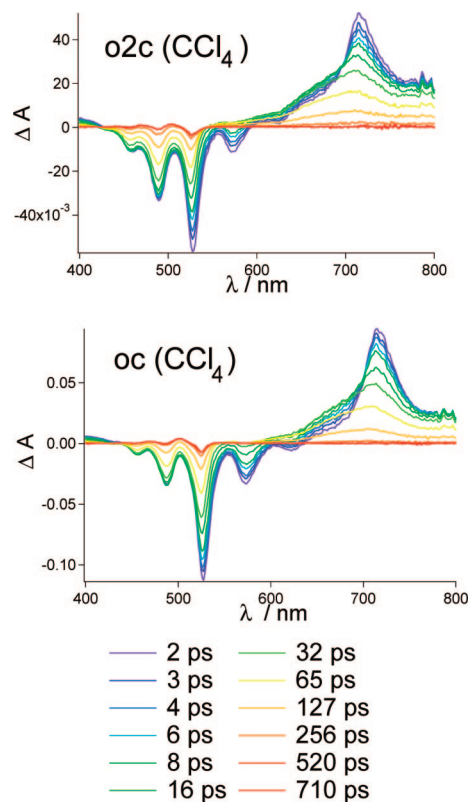


Figure 10. Femtosecond transient absorption spectra and corresponding time delays in CCl<sub>4</sub> after photoexcitation at 530 nm of compounds **o2c** (top) and **oc** (bottom). Note that, because of the low solubility of compound **o2c** in MCH, CCl<sub>4</sub> was instead chosen as the solvent of next lowest polarity.

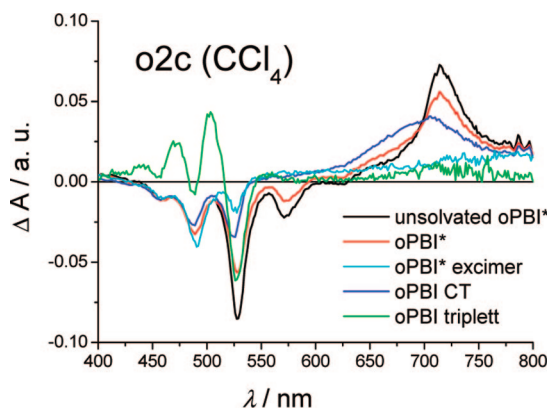
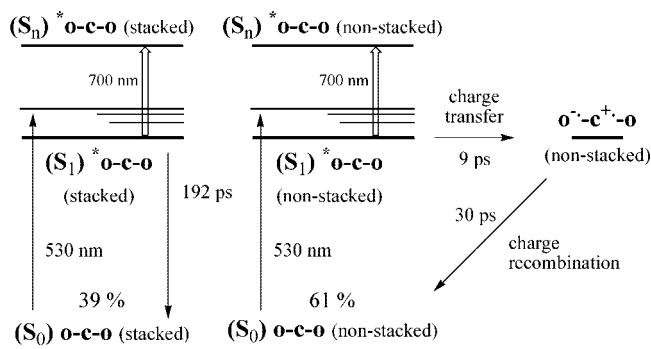


Figure 11. Species-associated difference spectra (SADS) of compound **o2c** in CCl<sub>4</sub> resulting from the global and target analysis of femtosecond transient absorption data employing the kinetic scheme depicted in Figure 12. Shown are processes after photoexcitation at 530 nm; features due to Raman scattering were omitted for clarity.

530 and 570 nm (stimulated emission of the orange PBI chromophore). Furthermore, a strong positive absorption band at 715 nm due to the singlet excited-state absorption of the orange perylene chromophore is found. Upon increasing solvent polarity, only slight changes in band shapes and general features of the spectra of the orange system **oc** (and of **oref** as well) have been observed in all other solvents (for spectra, we refer to Figures S16–S18 in the Supporting Information).<sup>24c,36</sup>

In contrast, for compound **o2c**, a strongly enhanced bleach signal at 485 nm is apparent in the spectra in CCl<sub>4</sub>, which is not found for solvents of higher polarity (see, for comparison, the spectra of compound **o2c** in toluene, CH<sub>2</sub>Cl<sub>2</sub>, and benzonitrile).



**Figure 12.** Energy level diagram of compound **o2c** in  $\text{CCl}_4$  showing deactivation pathways obtained with global and target analysis, together with the main decay times corresponding to the states.

trile in Figure S16). The band at 485 nm is attributed to the  $\pi$ -stacked pinched cone conformation of the calix[4]arene, and the femtosecond transient absorption spectra thus relate to the features already observed for the UV/vis absorption and fluorescence emission data.<sup>45</sup>

The femtosecond transients of the green and red dimers in various solvents do not give any indication for the formation of  $\pi$ -stacked systems (all spectra of monomers, dimers, and reference compounds in the various solvents are given in the Supporting Information, Figures S19–S24). The spectral features of very similar femtosecond transient absorption spectra have been extensively described.<sup>24c,d,46,14c</sup>

**Global and Target Analysis.** To further analyze the observed phenomena, the obtained data-matrices in the various solvents were analyzed with spectrotemporal parametrization.<sup>47</sup> As a final result, the so-called species associated difference spectra (SADS) are obtained, which reveal the lifetimes and also the true spectra of the individual excited-state species (see Figure 11). An elaborate example of spectrotemporal parametrization of calix[4]arene–PBI conjugates and further details of the method have been published recently.<sup>24c</sup>

For the data analysis of compound **o2c**, a kinetic scheme has been employed (see Figure 12) by assuming that both the  $\pi$ -stacked and nonstacked conformations being present in equilibrium in the ground state. The obtained SADS for compound **o2c** in  $\text{CCl}_4$  are depicted in Figure , and all other SADS are shown in Figure S25 in the Supporting Information. For compound **o2c** in  $\text{CCl}_4$ , five decay components are identified. The very first lifetime of 1.2 ps (black line in Figure 11) is attributed to fast solvent reorganization processes<sup>48</sup> (for comparison, see femtosecond transient absorption spectra of compound **oref** in Figure S18 in the Supporting Information). After 1.2 ps, two excited states are present that are attributed to the  $\pi$ -stacked and the nonstacked conformation, respectively (cyan and red lines in Figure 11, respectively). A lifetime of 192 ps is observed for the excited singlet state of the  $\pi$ -stacked excimer, and its SADS (cyan) shows the expected spectral patterns, i.e., a strongly enhanced bleach band at 490 nm, owing to the excited-state interaction of the two chromophoric PBI units. The SADS representing the excited-state of the nonstacked conformation (red) decays significantly faster within 9 ps forming a deactivation pathway via a charge transfer state involving the formation of the orange PBI monoanion (represented by the blue line in Figure 11). The latter SADS reveals a lifetime of 30 ps, and its spectral features show the complete loss of the stimulated emission at 580 nm and a significant broadening of the band at around 700 nm. This behavior has already been elucidated for compound **oc** and is due to a very

efficient photoinduced electron transfer process between the electron-poor orange PBI unit and the electron-rich calix[4]arene substituent.<sup>24c</sup> Furthermore, the detailed analysis of the late time gated spectra reveals that a small amount ( $<2\%$ ) of long-lived triplet is created for compound **o2c** (green line in Figure 11), which is also observed for compound **oc** (for details, see ref 24c).<sup>49</sup> Notably, much more efficient population of triplet states has recently been described for a related compound bearing two orange PBI chromophores tethered by a rigid xanthene spacer.<sup>50</sup>

For the target analysis of compound **o2c** in toluene (see Figure S25 in the Supporting Information), similar spectral species including those of the stacked pinched cone conformation are observed. Accordingly, in toluene, four decay components of 1.2 ps (fast solvent reorganization processes), 18 ps (excited-state decay for nonstacked chromophores), 53 ps (charge transfer state decay), and 111 ps (excimer decay) are found. The orange excimer state in toluene shows a smaller lifetime value of 111 ps compared to the one obtained in  $\text{CCl}_4$  of 192 ps because of the lower stabilization resulting from higher solvent polarity. Accordingly, this state is less stable in toluene, which relates to the findings from the steady-state optical properties. For both solvents  $\text{CH}_2\text{Cl}_2$  and benzonitrile, no spectral features attributable to the formation of an excimer-like state could be found by global analysis for the respective SADS. As already discussed for the time-resolved emission data, the observed lifetimes of the excimer state are significantly shorter than those for other PBI aggregates reported in the literature,<sup>42</sup> which is most likely due to the fast quenching of the excited-state of the orange PBI caused by the competitive photoinduced electron transfer process involving the calix[4]arene electron donor. For the green and red systems **g2c** and **r2c** in the various solvents, no excimer formation could be confirmed by global analysis, which again relates to the steady-state optical results.

## Conclusions

The calix[4]arene scaffold has been utilized to preorganize two orange, green, and red PBI chromophoric units, respectively. For the orange and green derivatives **o2c** and **g2c**, an equilibrium between the two possible pinched cone conformations of the calix[4]arene unit is observed, giving rise to the presence of a  $\pi$ -stacked conformation and a non- $\pi$ -stacked conformation. Our study shows that the amount of  $\pi$ -stacked pinched cone conformation in the equilibrium is affected by the substitution in the bay positions. With increased steric demand and the concomitant distortion of the chromophore out of planarity, the  $\pi$ -stacked conformation is destabilized, which is elaborated experimentally as well as by molecular modeling studies performed at the force-field level. We have shown that the two PBI units interact electronically in the  $\pi$ -stacked conformation, and hence the latter species exhibits spectral features known from sandwich-type aggregates with hypsochromically shifted absorption maxima and an excimer-type emission at long wavelength. Lowering the solvent polarity shifts the equilibrium toward the  $\pi$ -stacked form, and, accordingly, the amount of the  $\pi$ -stacked conformation is substantially increased in the solvents  $\text{CCl}_4$  and MCH.

Global and target analysis of the femtosecond transient absorption data is used for probing ground-state populations with excited-state dynamics. The molecules in the  $\pi$ -stacked conformation display a distinctly different decay behavior compared with the molecules in the nonstacked conformation. The former population decays via an excimer state, and the latter population decays through a charge separation process involving the calix[4]arene as electron donor.

**Acknowledgment.** We are grateful for financial support from the Deutsche Forschungsgemeinschaft (DFG) within the Graduiertenkolleg 1221 "Control of electronic properties of aggregated  $\pi$ -conjugated molecules", from the Nederlandse organisatie voor Wetenschappelijk Onderzoek (NWO) for the femtosecond equipment, and from the Universiteit van Amsterdam (UvA). The CNR staffs at ELETTRA (Trieste) are acknowledged for help in the use of the facility supported by CNR and by Elettra Scientific Division. C.H. is thankful to the Fonds der Chemischen Industrie for a Kekulé fellowship. The work in Mons is partly supported by the Interuniversity Attraction Pole program of the Belgian Federal Science Policy Office (PAI 6/27), by the EU through the Marie Curie Research Training Network THREADMILL (MRTN-CT-2006-036040) and by the Belgian National Science Foundation (FNRS/FRFC). D.B. is the research director of FNRS.

**Supporting Information Available:** Synthetic and experimental details, femtosecond transient absorption spectra and global and target analysis data. This material is available free of charge via the Internet at <http://pubs.acs.org>. Full crystallographic data of compound **r2c** have been deposited at the Cambridge Crystallographic Data Centre (CCDC reference number 687096).

## References and Notes

- (1) (a) *Calixarenes 2001*; Asfari, Z.; Böhmer, V.; Harrowfield, J., Eds.; Kluwer Academic Publishers: Dordrecht, 2001. (b) *Calixarenes*; Gutsche, C. D., Ed.; The Royal Society of Chemistry: Cambridge, U.K., 1993. (c) *Calixarenes Revisited*; Gutsche, C. D., Ed.; The Royal Society of Chemistry: Letchworth, U.K., 1998. (d) Böhmer, V. *Angew. Chem., Int. Ed. Engl.* **1995**, *34*, 713–745. (e) *Calixarenes in Action*; Mandolini, L.; Ungaro, R., Eds.; Imperial College Press: London, 2000.
- (2) Kenis, P. J. A.; Noordman, O. F. J.; Houbrechts, S.; van Hummel, G. J.; Harkema, S.; van Veggel, F. C. J. M.; Clays, K.; Engbersen, J. F. J.; Persoons, A.; van Hulst, N. F.; Reinhoudt, D. N. *J. Am. Chem. Soc.* **1998**, *120*, 7875–7883.
- (3) (a) Zhao, B.-T.; Blesa, M.-J.; Mercier, N.; Le Derf, F.; Sallé, M. *J. Org. Chem.* **2005**, *70*, 6254–6257. (b) Yu, H.-h.; Pullen, A. E.; Büschel, M. G.; Swager, T. M. *Angew. Chem., Int. Ed.* **2004**, *43*, 3700–3703. (c) Yu, H.-h.; Xu, B.; Swager, T. M. *J. Am. Chem. Soc.* **2003**, *125*, 1142–1143. (d) Scherlis, D. A.; Marzari, N. *J. Am. Chem. Soc.* **2005**, *127*, 3207–3212.
- (4) (a) Schazmann, B.; Alhashimy, N.; Diamond, D. *J. Am. Chem. Soc.* **2006**, *128*, 8607–8614. (b) Souchon, V.; Leray, I.; Valeur, B. *Chem. Commun.* **2006**, 4224–4226. (c) Lee, S. H.; Kim, S. H.; Kim, S. K.; Jung, J. H.; Kim, J. S. *J. Org. Chem.* **2005**, *70*, 9288–9295. (d) Leray, I.; Lefevre, J.-P.; Delouis, J.-F.; Delaire, J.; Valeur, B. *Chem.—Eur. J.* **2001**, *7*, 4590–4598. (e) van der Veen, N.; Flink, S.; Deij, M. A.; Egberink, R. J. M.; van Veggel, F. C. J. M.; Reinhoudt, D. N. *J. Am. Chem. Soc.* **2000**, *122*, 6112–6113. (f) Ji, H.-F.; Dabestani, R.; Brown, G. M.; Sachleben, R. A. *Chem. Commun.* **2000**, 833–834. (g) Beer, P. D.; Timoshenko, V.; Maestri, M.; Passaniti, P.; Balzani, V. *Chem. Commun.* **1999**, 1755–1756. (h) Jin, T.; Monde, K. *Chem. Commun.* **1998**, 1357–1358. (i) Aoki, I.; Sakaki, T.; Shinkai, S. *J. Chem. Soc., Chem. Commun.* **1992**, 730–732. (j) Jin, T.; Ichikawa, K.; Koyama, T. *J. Chem. Soc., Chem. Commun.* **1992**, 499–501.
- (5) (a) Araki, K.; Iwamoto, K.; Shinkai, S.; Matsuda, T. *Chem. Lett.* **1989**, 1747–1750. (b) Iwamoto, K.; Araki, K.; Shinkai, S. *J. Org. Chem.* **1991**, *56*, 4955–4962.
- (6) (a) Conner, M.; Janout, V.; Regen, S. L. *J. Am. Chem. Soc.* **1991**, *113*, 9670–9671. (b) Scheerder, J.; Vreekamp, R. H.; Engbersen, J. F. J.; Verboom, W.; van Duynhoven, J. P. M.; Reinhoudt, D. N. *J. Org. Chem.* **1996**, *61*, 3476–3481. (c) Grootenhuis, P. D. J.; Kollman, P. A.; Groenen, L. C.; Reinhoudt, D. N.; van Hummel, G. J.; Ugozzoli, F.; Andreotti, G. D. *J. Am. Chem. Soc.* **1990**, *112*, 4165–4176. (d) Harada, T.; Rudzinski, J. M.; Osawa, E.; Shinkai, S. *Tetrahedron Lett.* **1993**, *49*, 5941–5954.
- (7) (a) Arduini, A.; Fabbri, M.; Mirone, L.; Pochini, A.; Secchi, A.; Ungaro, R. *J. Org. Chem.* **1995**, *69*, 1454–1457. (b) Ikeda, A.; Tsuzuki, K.; Shinkai, S. *J. Chem. Soc., Perkin Trans. 2* **1994**, 2073–2080. (c) Timmerman, P.; Nierop, K. G. A.; Brinks, E. A.; Verboom, W.; van Veggel, F. C. J. M.; van Hoorn, W. P.; Reinhoudt, D. N. *Chem.—Eur. J.* **1995**, *1*, 132–143. (d) Matoušek, J.; Kulhánek, P.; Čajan, M.; Koča, J. *J. Phys. Chem. A* **2006**, *110*, 861–867.
- (8) Würthner, F. *Chem. Commun.* **2004**, 1564–1579.
- (9) (a) *Supramolecular Chemistry: Concepts and Perspectives*; Lehn, J.-M., Ed.; VCH: Weinheim, Germany, 1995. (b) *Supramolecular Dye Chemistry*; Würthner, F., Ed.; Topics in Current Chemistry 258, Springer-Verlag: Berlin, 2005.
- (10) (a) Hoeben, F. J. M.; Jonkheijm, P.; Meijer, E. W.; Schenning, A. P. H. *J. Chem. Rev.* **2005**, *105*, 1491–1546. (b) Simpson, C. D.; Wu, J.; Watson, M. D.; Müllen, K. *J. Mater. Chem.* **2004**, *14*, 494–504. (c) Würthner, F.; Thalacker, C.; Diele, S.; Tschierske, C. *Chem.—Eur. J.* **2001**, *7*, 2245–2253.
- (11) You, C.-C.; Dobrawa, R.; Saha-Möller, C. R.; Würthner, F. *Top. Curr. Chem.* **2005**, *258*, 39–82.
- (12) (a) Ford, W. E.; Kamat, P. V. *J. Phys. Chem.* **1987**, *91*, 6373–6380. (b) Gvishli, R.; Reisfeld, R.; Burshtein, Z. *Chem. Phys. Lett.* **1993**, *213*, 338–344.
- (13) (a) De Schryver, F. C.; Vosch, T.; Cotlet, M.; Van der Auweraer, M.; Müllen, K.; Hofkens, J. *Acc. Chem. Res.* **2005**, *38*, 514–522. (b) Sautter, A.; Kaletas, B. K.; Schmid, D. G.; Dobrawa, R.; Zimine, M.; Jung, G.; Van Stokkum, I. H. M.; De Cola, L.; Williams, R. M.; Würthner, F. *J. Am. Chem. Soc.* **2005**, *127*, 6719–6729.
- (14) (a) O'Neil, M. P.; Niemczyk, M. P.; Svec, W. A.; Gosztola, D.; Gaines, G. L., III; Wasielewski, M. R. *Science* **1992**, *257*, 63–65. (b) Beckers, E. H. A.; Meskers, S. C. J.; Schenning, A. P. H. J.; Chen, Z.; Würthner, F.; Janssen, R. A. J. *J. Phys. Chem. A* **2004**, *108*, 6933–6937. (c) Prodi, A.; Chiorboli, C.; Scandola, F.; Iengo, E.; Alessio, E.; Dobrawa, R.; Würthner, F. *J. Am. Chem. Soc.* **2005**, *127*, 1454–1462.
- (15) (a) Kraft, A.; Grimsdale, A. C.; Holmes, A. B. *Angew. Chem., Int. Ed.* **1998**, *37*, 402–428. (b) Karapire, C.; Zafer, C.; Icli, S. *Synth. Met.* **2004**, *145*, 51–60. (c) Pan, J.; Zhu, W.; Li, S.; Zeng, W.; Cao, Y.; Tian, H. *Polymer* **2005**, *46*, 7658–7669.
- (16) (a) Malenfant, P. R. L.; Dimitrakopoulos, C. D.; Gelorme, J. D.; Kosar, L. L.; Graham, T. O. *Appl. Phys. Lett.* **2002**, 2517–2519. (b) Dimitrakopoulos, C. D.; Malenfant, P. R. L. *Adv. Mater.* **2002**, *14*, 99–117. (c) Jones, B. A.; Ahrens, M. J.; Yoon, M.-H.; Facchetti, A.; Marks, T. J.; Wasielewski, M. R. *Angew. Chem., Int. Ed.* **2004**, *116*, 6363–6366. (d) Würthner, F.; Schmidt, R. *ChemPhysChem* **2006**, *7*, 793–797.
- (17) (a) Tang, C. W. *Appl. Phys. Lett.* **1986**, *48*, 183–185. (b) Schmidt-Mende, L.; Fechtenkötter, A.; Müllen, K.; Moons, E.; Friend, R. H.; MacKenzie, J. D. *Science* **2001**, *293*, 1119–1122. (c) Breeze, A. J.; Salomon, A.; Ginley, D. S.; Gregg, B. A.; Tillmann, H.; Hörhold, H.-H. *Appl. Phys. Lett.* **2002**, *81*, 3085–3087.
- (18) Seybold, G.; Stange, A. (BASF AG), Ger. Pat. DE 35 45 004, 1987 (*Chem. Abstr.* **1988**, *108*, 77134c).
- (19) Zhao, Y.; Wasielewski, M. R. *Tetrahedron Lett.* **1999**, *40*, 7047–7050.
- (20) Langhals, H. *Heterocycles* **1995**, *40*, 477–500.
- (21) For examples with rigid spacer units containing PBIs, see (a) Giaimo, J. M.; Gusev, A. V.; Wasielewski, M. R. *J. Am. Chem. Soc.* **2002**, *124*, 8530–8531. (b) Ahrens, M. J.; Sinks, L. E.; Rytchinski, B.; Liu, W.; Jones, B. A.; Giaimo, J. M.; Gusev, A. V.; Goshe, A. J.; Tiede, D. M.; Wasielewski, M. R. *J. Am. Chem. Soc.* **2004**, *126*, 8284–8294. (c) Rytchinski, B.; Sinks, L. E.; Wasielewski, M. R. *J. Phys. Chem. A* **2004**, *108*, 7497–7505. (d) Van der Boom, T.; Hayes, R. T.; Zhao, Y.; Bushard, P. J.; Weiss, E. A.; Wasielewski, M. R. *J. Am. Chem. Soc.* **2002**, *124*, 9582–9590. (e) Giaimo, J. M.; Lockard, J. V.; Sinks, L. E.; Scott, A. M.; Wilson, T. M.; Wasielewski, M. R. *J. Phys. Chem. A* **2008**, *112*, 2322–2330.
- (22) For other bis-chromophoric systems, see (a) Jokic, D.; Asfari, Z.; Weiss, J. *Org. Lett.* **2002**, *4*, 2129–2132. (b) Yu, H.-H.; Pullen, A. E.; Büschel, M. G.; Swager, T. M. *Angew. Chem., Int. Ed.* **2004**, *43*, 3700–3703. (c) Kadish, K. M.; Frémond, L.; Ou, Z.; Shao, J.; Shi, C.; Anson, F. C.; Burdet, F.; Gros, C. P.; Barbe, J.-M.; Guillard, R. *J. Am. Chem. Soc.* **2005**, *127*, 5625–5631. (d) Scherlis, A. S.; Marzari, N. *J. Am. Chem. Soc.* **2005**, *127*, 3207–3212. (e) Pognon, G.; Boudon, C.; Schenk, K. J.; Bonin, M.; Bach, B.; Weiss, J. *J. Am. Chem. Soc.* **2006**, *128*, 3488–3489. (f) Van der Boom, T.; Evmenenko, G.; Dutta, P.; Wasielewski, M. R. *Chem. Mater.* **2003**, *15*, 4068–4074.
- (23) (a) Neuteboom, E. E.; Meskers, S. C. J.; Meijer, E. W.; Janssen, R. A. J. *Macromol. Chem. Phys.* **2004**, *205*, 217–222. (b) Wang, W.; Wan, W.; Zhou, H.-H.; Niu, S.; Li, A. D. Q. *J. Am. Chem. Soc.* **2003**, *125*, 5248–5249. (c) Wang, W.; Li, L.-S.; Helms, G.; Zhou, H.-H.; Li, A. D. Q. *J. Am. Chem. Soc.* **2003**, *125*, 1120–1121. (d) Hernando, J.; De Witte, P. A. J.; Van Dijk, E. M. H. P.; Korterik, J.; Nolte, R. J. M.; Rowan, A. E.; Garcia-Parajó, M. F.; Van Hulst, N. F. *Angew. Chem., Int. Ed.* **2004**, *43*, 4045–4049. (e) Staab, H. A.; Riegler, N.; Diederich, F.; Krieger, C.; Schweitzer, D. *Chem. Ber.* **1984**, *117*, 246–259. (f) Langhals, H.; Ismael, R. *Eur. J. Org. Chem.* **1998**, 1915–1917.
- (24) (a) Hippus, C.; Schlosser, F.; Vysotsky, M. O.; Böhmer, V.; Würthner, F. *J. Am. Chem. Soc.* **2006**, *128*, 3870–3871. (b) Vysotsky, M. O.; Böhmer, V.; Würthner, F.; You, C.-C.; Rissanen, K. *Org. Lett.* **2002**, *4*, 2901–2904. (c) Hippus, C.; van Stokkum, I. H. M.; Zangrando, E.; Williams, R. M.; Würthner, F. *J. Phys. Chem. C* **2007**, *111*, 13988–13996. (d) Hippus, C.; van Stokkum, I. H. M.; Gsänger, M.; Groeneveld, M. M.; Williams, R. M.; Würthner, F. *J. Phys. Chem. C* **2008**, *112*, 2476–2486.

(25) (a) Osswald, P.; Leusser, D.; Stalke, D.; Würthner, F. *Angew. Chem., Int. Ed.* **2005**, *44*, 250–253. (b) Osswald, P.; Würthner, F. *Chem.—Eur. J.* **2007**, *13*, 7395–7409.

(26) Measurements were performed in the range from 273 to 334 K for compounds **o2c** and **g2c**, and in the range from 273 to 325 K for compound **r2c**. Because of precipitation of the compounds in MCH, CCl<sub>4</sub> was instead chosen as the solvent. As a consequence, the accessible lower temperature range is limited by the melting point of CCl<sub>4</sub>.

(27) Osswald, P.; Würthner, F. *J. Am. Chem. Soc.* **2007**, *129*, 14319–14326.

(28) Kasha, M.; Rawls, H. R.; El-Bayoumi, M. A. *Pure Appl. Chem.* **1965**, *11*, 371–392.

(29) (a) *Electronic Processes in Organic Crystals and Polymers*; Pope, M.; Swenberg, C. E.; Oxford University Press: New York, 1999. (b) Kazmaier, P. M.; Hoffmann, R. H. *J. Am. Chem. Soc.* **1994**, *116*, 9684–9691.

(30) For examples containing PBI dyes, see refs 21, 23f, and (a) Li, X.; Sinks, L. E.; Rybtchinski, B.; Wasielewski, M. R. *J. Am. Chem. Soc.* **2004**, *126*, 10810–10811. (b) Langhals, H.; Jona, W. *Angew. Chem., Int. Ed.* **1998**, *37*, 952–955. (c) Li, A. D. Q.; Wang, W.; Wang, L.-Q. *Chem.—Eur. J.* **2003**, *9*, 4594–4601.

(31) Würthner, F.; Ahmed, S.; Thalacker, C.; Debaerdemaeker, T. *Chem.—Eur. J.* **2002**, *20*, 4742–4750.

(32) Chen, Z.; Stepanenko, V.; Dehm, V.; Prins, P.; Siebbeles, L. D. A.; Seibt, J.; Marquetand, P.; Engel, V.; Würthner, F. *Chem.—Eur. J.* **2007**, *13*, 436–449.

(33) Note that CCl<sub>4</sub> was chosen as a solvent because precipitation of compounds **o2c** and **g2c** is observed after approximately 30 min for the solution of both **o2c** and **g2c** in MCH, respectively.

(34) Notably, all UV/vis absorption spectra show a small blue shift with increasing temperature, and a slightly reduced peak intensity for the absorption maximum. These spectral changes are observed for both the monomeric and dimeric series as well as for the respective reference compounds without calix[4]arene substitution (see Figures S12 and S13 in the Supporting Information). Hence, the observed effects appear to be independent of the respective PBI unit as well as the calix[4]arene substitution on the chromophore. We attribute the hypsochromic shift to a decrease of the dielectric constant of CCl<sub>4</sub> with increasing temperature,<sup>35</sup> and the reduced absorption coefficient is attributed to the broadening of the absorption band due to the population of more conformations at higher temperature.

(35) This is supported by the fact that, for compound **oref**, a hypsochromic shift of the band maximum from 523 nm in CCl<sub>4</sub> (with a relative permittivity of  $\epsilon@293\text{ K} = 2.24$ ) to 517 nm ( $\epsilon@293\text{ K} = 2.02$ ) in MCH is observed. Hence, lowering the solvent polarity of  $\Delta\epsilon \approx 0.2$  leads to a spectral shift of about 6 nm. For the permittivity of CCl<sub>4</sub> at 343 K, a value of  $\epsilon = 2.14$  is given, and, accordingly, an increase of temperature between 293 and 343 K leads to a reduced permittivity of  $\Delta\epsilon \approx 0.1$ , resulting in a hypsochromic shift of the band maximum of 3 nm from 523 nm ( $T = 293\text{ K}$ ) to 520 nm ( $T = 343\text{ K}$ ). Similar behavior is also found for compound **gref** (with 17 nm shift upon solvent change with  $\Delta\epsilon \approx 0.2$ , and with 8 nm shift upon temperature change with  $\Delta\epsilon \approx 0.1$ ) and compound **rref** (with 11 nm shift upon solvent change with  $\Delta\epsilon \approx 0.2$ , and with 5 nm shift upon temperature change with  $\Delta\epsilon \approx 0.1$ ). For temperature-dependent permittivity values, see *CRC Handbook of Chemistry and Physics*, 76th ed.; Lide, D. R., Ed.; CRC Press: Boca Raton, FL, 1995.

(36) Note, that because of a very efficient photoinduced electron transfer process ( $k_{CT} = 3.1 \times 10^{10}\text{ s}^{-1}$  in CH<sub>2</sub>Cl<sub>2</sub>) between the electron-poor orange PBI unit and the electron-rich calix[4]arene substituent, the quantum yield of the orange PBI chromophore is strongly quenched for both calix[4]arene-substituted compounds **o2c** and **oc**, respectively, already for the non-

aggregate species.<sup>24c</sup> In contrast, the orange reference compound **oref** reveals quantum yields of almost unity in all five solvents (see Table 1).

(37) (a) Case, D. A.; Darden, T. A.; Cheatham, T. E., III; Simmerling, C. L.; Wang, J.; Duke, R. E.; Luo, R.; Merz, K. M.; Pearlman, D. A.; Crowley, M.; Walker, R. C.; Zhang, W.; Wang, B.; Hayik, S.; Roitberg, A.; Seabra, G.; Wong, K. F.; Paesani, F.; Wu, X.; Brozell, S.; Tsui, V.; Gohlke, H.; Yang, L.; Tan, C.; Mongan, J.; Hornak, V.; Cui, G.; Beroza, P.; Matthews, D. H.; Schafmeister, C.; Ross, W. S.; Kollman, P. A. *AMBER 9*; University of California: San Francisco, 2006. (b) Pearlman, D. A.; Case, D. A.; Caldwell, J. W.; Ross, W. S.; Cheatham, T. E., III; De Bolt, S.; Ferguson, D.; Seibel, G.; Kollman, P. *Comput. Phys. Commun.* **1995**, *91*, 1–41. (c) Case, D. A.; Cheatham, T.; Darden, T.; Gohlke, H.; Luo, R., Jr.; Onufriev, A.; Simmerling, C.; Wang, B.; Woods, R. J. *J. Comput. Chem.* **2005**, *26*, 1668–1688.

(38) Wang, J.; Wolf, R. M.; Caldwell, J. W.; Kollman, P. A.; Case, D. A. *J. Comput. Chem.* **2004**, *25*, 1157–1174.

(39) Jakalian, A.; Bush, B. L.; Jack, D. B.; Bayly, C. I. *J. Comput. Chem.* **2000**, *21*, 132–146.

(40) Ridley, J.; Zerner, M. C. *Theor. Chim. Acta* **1973**, *32*, 111.

(41) Hennebicq, E.; Pourtois, G.; Scholes, G. D.; Herz, L. M.; Russell, D. M.; Silva, C.; Setayesh, S.; Grimsdale, A. C.; Müllen, K.; Brédas, J.-L.; Beljonne, D. *J. Am. Chem. Soc.* **2005**, *127*, 4744.

(42) Longer-lived excited states due to PBI-excimer formation have been reported in the literature; see (a) Katoh, R.; Sinha, S.; Murata, S.; Tachiya, M. *J. Photochem. Photobiol., A* **2001**, *145*, 23–34. (b) Gómez, U.; Leonhardt, M.; Port, H.; Wolf, H. C. *Chem. Phys. Lett.* **1997**, *268*, 1–6. (c) Puech, K.; Fröb, H.; Leo, K. *J. Lumin.* **1997**, *72–74*, 524–525.

(43) For all lifetimes determined for compounds **g2c**, **gc**, and **gref**, biexponential decays are observed. Accordingly, additional small components of ca. 0.5 ns are found for each compound independent of the solvent polarity and of the calix[4]arene substitution of the chromophore. The latter components are thus considered to be independent of the calix[4]arene substitution of the dye unit and are inherent to the green PBI chromophore itself (for details refer to Table 3).

(44) Ford, W. E.; Hiratsuka, H.; Kamat, P. V. *J. Phys. Chem.* **1989**, *93*, 6692–6696.

(45) Solutions of **o2c** and **oc** in the lowest polarity solvent MCH could not be measured due to precipitation of the compounds.

(46) (a) Lukas, A. S.; Zhao, Y.; Miller, S. E.; Wasielewski, M. R. *J. Phys. Chem. B* **2002**, *106*, 1299–1306. (b) Shibano, Y.; Umeiyama, T.; Matano, Y.; Tkachenko, N. V.; Lemmetyinen, H.; Imahori, H. *Org. Lett.* **2006**, *8*, 4425–4428.

(47) (a) van Stokkum, I. H. M.; Larsen, D. S.; van Grondelle, R. *Biochim. Biophys. Acta* **2004**, *1657*, 82–104. (b) van Stokkum, I. H. M.; Lozier, R. H. *J. Phys. Chem. B* **2002**, *106*, 3477–3485. (c) Mullen, K. M.; van Stokkum, I. H. M. *J. Stat. Software* **2007**, *18* (3). URL: <http://www.jstatsoft.org/v18/i03/>. (d) Global and target analysis can be performed with, e.g., the R package TIMP; see <http://cran.r-project.org/doc/packages/TIMP.pdf>.

(48) (a) Schweitzer, G.; Gronheid, R.; Jordens, S.; Lor, M.; De Belder, G.; Weil, T.; Reuther, E.; Müllen, K.; De Schryver, F. C. *J. Phys. Chem. A* **2003**, *107*, 3199–3207. (b) De Belder, G.; Jordens, S.; Lor, M.; Schweitzer, G.; De, R.; Weil, T.; Herrmann, A.; Wiesler, U. K.; Müllen, K.; De Schryver, F. C. *J. Photochem. Photobiol. A* **2001**, *145*, 61–70.

(49) An excited-state charge transfer process resulting in a charge transfer state of the  $\pi$ -stacked form could not be unambiguously confirmed by global and target analysis.

(50) Veldman, D.; Chopin, S. M. A.; Meskers, S. C. J.; Groeneveld, M. M.; Williams, R. M.; Janssen, R. A. J. *J. Phys. Chem. A* **2008**, *112*, 5846.

JP804068B